

Three-Loop Neutrino Mass Models at Colliders

Amine Ahriche ^{1,2}, Kristian L. McDonald ³ & Salah Nasri ⁴

¹ *Department of Physics, University of Jijel, PB 98 Ouled Aissa, DZ-18000 Jijel, Algeria*

² *The Abdus Salam International Centre for Theoretical Physics, Strada Costiera 11, I-34014, Trieste, Italy*

³ *ARC Centre of Excellence for Particle Physics at the Terascale, School of Physics, The University of Sydney, NSW 2006, Australia.*

⁴ *Physics Department, UAE University, POB 17551, Al Ain, United Arab Emirates*



In this work, we report on recent analyses of a class of models that generate neutrino mass at the three-loop level. We argue that these models offer a viable solution to both the neutrino mass and dark matter problems, without being in conflict with experimental constraints from, e.g. lepton flavor violating processes and the muon anomalous magnetic moment. Furthermore, we describe observable experimental signals predicted by the models and show that they have common signatures that can be probed at both the LHC and ILC.

1 Introduction

The Standard Model has been remarkably successful in describing physics at the weak scale. However, many questions remain, including those relating to the origin of neutrino mass and the reason for its smallness. In this context, models with radiative neutrino mass are of significant experimental interest. These models provide an inherent loop-suppression that allows the new physics responsible for neutrino mass to be lighter than in other scenarios. This loop suppression is more severe as the number of loops increases, making models with three-loop masses particularly interesting, as they generically require new physics near the TeV scale. Such light new particles can be produced and detected within current and near-future experiments by searching for signatures such as lepton flavor violating (LFV) effects.

Here we present a class of models with common features, in which neutrino mass is generated at the three-loop level ^{1,2,3,4,5}, and discuss interesting signatures that can appear at both leptonic and hadronic colliders. We focus primarily on the KNT model ¹ and present recent analyses showing that the model satisfies LFV constraints, such as $\mu \rightarrow e + \gamma$, and fits the neutrino oscillation data. Furthermore, the model contains a viable candidate for the dark matter (DM) in the universe, in the form of a light right-handed (RH) neutrino. We also show that a strongly first order electroweak phase transition can be achieved with a Higgs mass of $\simeq 125$ GeV, as measured at the LHC ^{6,7}. The model contains new charged scalars that may lead to significant modification on the Higgs decay channel $h \rightarrow \gamma\gamma$ while $h \rightarrow \gamma\gamma$ remains SM-like. We also discuss possible signature of this class of models at the ILC and LHC through possible modifications of the processes $e^-e^+ \rightarrow e^-\mu^+ + E_{miss}$ and $pp \rightarrow e^-e^+ + E_{miss}$, $\mu^-\mu^+ + E_{miss}$, $e^-\mu^+ + E_{miss}$ respectively.

2 A Class of Three-Loop Models

The class of models we discuss is based on the KNT model ¹, which is obtained by extending the SM to include three right-handed (RH) Majorana neutrinos and two electrically charged

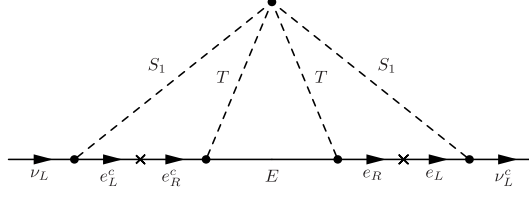


Figure 1: The three-loop diagram that generates the neutrino mass.

scalars, S_1^\pm and S_2^\pm , all of which are singlets under $SU(2)_L$. In addition, a discrete Z_2 symmetry is imposed, under which $\{S_2, N_i\} \rightarrow \{-S_2, -N_i\}$, and all other fields are even. The generalized class of models is obtained by promoting the charged scalar S_2^\pm to a scalar multiplet T , and the three RH neutrinos N_i to three generations of fermionic multiplets E_i , while retaining the same charges under the Z_2 symmetry^a. This symmetry plays two key roles, preventing a tree-level coupling between N_R (E_i) and the SM Higgs, which would otherwise induce tree-level neutrino masses, and ensuring that the lightest neutral fermion E_i^0 is a stable DM candidate. The general Lagrangian reads as

$$\mathcal{L} = \mathcal{L}_{SM} + \{f_{\alpha\beta} L_\alpha^T C i \tau_2 L_\beta S_1^+ + g_{i\alpha} \bar{E}_i T \ell_{\alpha R} - \frac{1}{2} \bar{E}_i^c M_{ij} E_j + h.c\} - V, \quad (1)$$

where L_α is the left-handed lepton doublet, $f_{\alpha\beta}$ are Yukawa couplings which are antisymmetric in the generation indices α and β , M_{ij} are the fermionic mass matrix elements, C is the charge conjugation matrix, and $V(\Phi, S_1, T)$ is the tree-level scalar potential. Here Φ denotes the SM Higgs doublet.

Using interactions in (1) together with the scalar interaction $V \supset \lambda_s S_1^+ S_1^- T^\dagger T$, the neutrino mass matrix elements can arise from the three-loop diagram in Fig. 1, that are given by⁸

$$(M_\nu)_{\alpha\beta} = \frac{(2n+1)\lambda_s m_{\ell_i} m_{\ell_k}}{(4\pi^2)^3 M_T} f_{\alpha i} f_{\beta k} g_{ij} g_{kj} F\left(M_{E_j}^2/M_T^2, M_{S_1}^2/M_T^2\right), \quad (2)$$

where $\rho, \kappa (= e, \mu, \tau)$ are the charged leptons flavor indices, $i = 1, 2, 3$ denotes the three E_i multiplets, and the function F is a loop integral which is $\mathcal{O}(1)$ ⁸. It is interesting to note that, unlike the conventional seesaw mechanism, the radiatively generated neutrino masses are directly proportional to the charged lepton and RH neutrino masses, as well as being loop-suppressed. Here $n = 0$ corresponds to the KNT model, while $n = 1, 2, 3$ gives generalizations where E_i and T are $SU(2)_L$ triplets, quintuplets and septuplets, respectively (i.e. T and E_i are both assigned to the $(2n+1)$ representation under $SU(2)_L$ and carry two units of hypercharge).

The Lagrangian (1) induces flavor violating processes, such as $\ell_\alpha \rightarrow \gamma \ell_\beta$ for $m_{\ell_\alpha} > m_{\ell_\beta}$, and an extra contribution to the muon anomalous magnetic moment. Both are generated at one loop via the exchange of the charged scalar S_1^\pm , and the members of the multiplets T and E_i . The LFV branching ratios and the muon anomalous magnetic moment are given by

$$B(\ell_\alpha \rightarrow \gamma \ell_\beta) = \frac{3\alpha_{em} v^4}{36\pi} \left\{ \frac{|f_{\kappa\alpha} f_{\kappa\beta}^*|^2}{36M_{S_1}^4} + \frac{(2n+1)^2}{M_T^4} \left| \sum_i g_{i\alpha} g_{i\beta}^* F_2(M_{E_i}^2/M_T^2) \right|^2 \right\}, \quad (3)$$

$$\delta a_\mu = -\frac{m_\mu^2}{16\pi^2} \left\{ \sum_{\alpha \neq \mu} \frac{|f_{\mu\alpha}|^2}{6M_{S_1}^2} + n \sum_i \frac{|g_{i\mu}|^2}{M_T^2} F_2(M_{E_i}^2/M_T^2) \right\}, \quad (4)$$

with $\kappa \neq \alpha, \beta$, α_{em} being the fine structure constant and $F_2(x) = (1 - 6x + 3x^2 + 2x^3 - 6x^2 \ln x)/6(1-x)^4$.

^aExcept for the septuplet case where the global symmetry Z_2 is accidental⁴.

In our scan of the parameter space of the model we impose the experimental bounds on $B(\mu \rightarrow e\gamma)$ ⁹, $B(\tau \rightarrow \mu\gamma)$ and δa_μ ¹⁰, and use the allowed values for the neutrino mixing parameters, $s_{12}^2 = 0.320^{+0.016}_{-0.017}$, $s_{23}^2 = 0.43^{+0.03}_{-0.03}$, $s_{13}^2 = 0.025^{+0.003}_{-0.003}$, and the mass squared differences, $|\Delta m_{31}^2| = 2.55^{+0.06}_{-0.09} \times 10^{-3} \text{ eV}^2$ and $\Delta m_{21}^2 = 7.62^{+0.19}_{-0.19} \times 10^{-5} \text{ eV}^2$ ¹¹.

3 Dark Matter

An immediate implication of the Z_2 symmetry is that that lightest neutral fermion, E_1^0 , is stable, and hence a candidate for dark matter (DM). The E_1^0 number density gets depleted through the process $E_1^0 E_1^0 \rightarrow \ell_\alpha \ell_\beta$ via the t - and u -channel exchange of T . In the singlet case ($n = 0$), the non-relativistic limit of the annihilation cross section gives

$$\sigma_{E_1^0 E_1^0} v_r \simeq \sum_{\alpha, \beta} |g_{1\alpha} g_{1\beta}^*|^2 \frac{M_{E_1}^2 (M_T^4 + M_{E_1}^4)}{48\pi (M_T^2 + M_{E_1}^2)^4} v_r^2, \quad (5)$$

with v_r is the relative velocity between the annihilation E_1^0 's. In cases with nontrivial representations ($n \neq 0$), there exist other annihilation channels, such as $E_1^0 E_1^0 \rightarrow WW$, which increase the annihilation cross section, and therefore the DM candidate should be heavier. The WW annihilation cross section contribution is given by

$$\sigma_{E_1^0 E_1^0 \rightarrow WW} v_r = \frac{\pi \alpha_2^2}{M_{E_1}^2} (a + b v_r^2), \quad (6)$$

with the $SU(2)_L$ structure constant $\alpha_2 = g^2/4\pi$; and $\{a, b\} = \{\frac{37}{12}, \frac{17}{48}\}$, $\{\frac{207}{20}, \frac{243}{80}\}$, $\{\frac{174}{7}, \frac{263}{28}\}$ for $n = 1, 2, 3$ respectively.

When combining the relic density together with the neutrino mass and mixing, LFV and muon anomalous magnetic moment bounds, the mass of the charged scalar S_1 should exceed 100 GeV, while the bounds on E_i and T are sensitive to the $SU(2)_L$ quantum numbers. For the KNT case ($n=0$), we find that $M_{E_1^0} < 225 \text{ GeV}$ while $M_T < 245 \text{ GeV}$ ⁸. For the triplet, quintuplet and septuplet cases the DM mass should be in the ranges $M_{E_1^0} = 2.35 \sim 2.75 \text{ TeV}$ ², $M_{E_1^0} \sim 6 \text{ TeV}$ ³ and $M_{E_1^0} \sim 21 \text{ TeV}$ ⁴ respectively, with $M_T > M_{E_1^0}$.

4 Electroweak Phase Transition

Although the SM has all the qualitative ingredients for electroweak baryogenesis, the amount of matter-antimatter asymmetry generated is too small. One of the reasons for this smallness is the fact that the electroweak phase transition (EWPT) is not strongly first order, which is necessary to suppress the sphaleron processes in the broken phase. The EWPT strength can be improved if new scalar degrees of freedom around the electroweak scale are coupled to the SM Higgs, which is the case in this class of models.

The investigation of the scalar effective potential reveals that, within the allowed parameter space of the model, the strength of the electroweak phase transition (EWPT) can be first order⁸. We found that if the one-loop corrections to the Higgs mass are sizeable, then the strongly first order EWPT condition, $v(T_c)/T_c > 1$, can be realized while keeping the Higgs mass around 125 GeV. The reason for this being that the extra charged singlets affect the dynamics of the SM scalar field VEV around the critical temperature¹².

The existence of extra fields coupled to SM Higgs doublet will induce one-loop corrections to the triple Higgs coupling, $\lambda_{hhh}^{(3)}$, which is of great interest, especially at leptonic colliders. In Fig. 2-left, we show the plot for $v(T_c)/T_c$ versus the critical temperature. One observes that a strongly first order EWPT is possible while the critical temperature lies around 100 GeV. In Fig. 2-right, we show the ratio $v(T_c)/T_c$ versus the relative enhancement on the triple Higgs

coupling due to new physics, $\Delta = (\lambda_{hhh}^{(3)} - \lambda_{hhh}^{SM}) / \lambda_{hhh}^{SM}$. It is clear that the enhancement is significant when the EWPT is stronger.

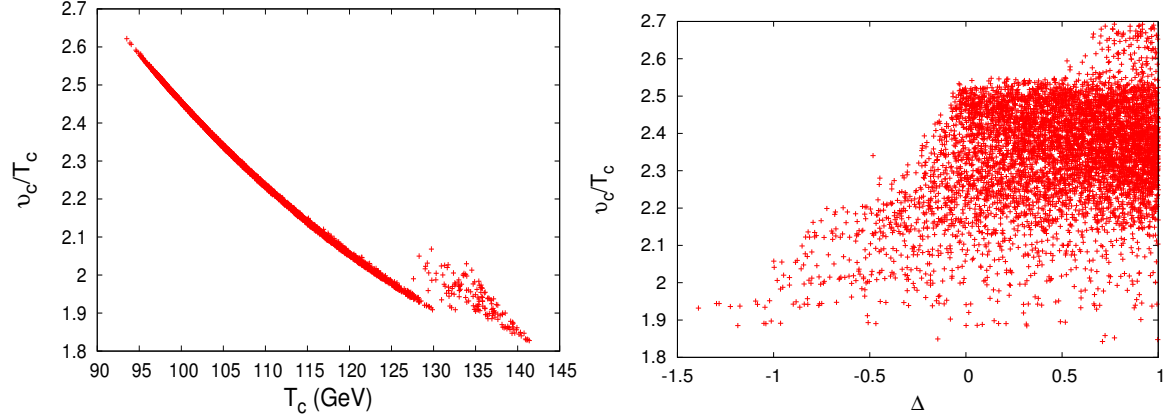


Figure 2: Left: the critical temperature is presented versus the quantity v_c/T_c . Right: the ratio v_c/T_c versus the relative enhancement in the Higgs triple coupling $\Delta = (\lambda_{hhh}^{(3)} - \lambda_{hhh}^{SM}) / \lambda_{hhh}^{SM}$.

5 Collider Phenomenology

In these models, there are many common signatures at both the ILC and LHC. Here, we briefly discuss two common signals, one at the ILC and another at the LHC. At the ILC, the process $e^-e^+ \rightarrow e^-\mu^+ + E_{miss}$ is modified in this class of models, where $E_{miss} \equiv \nu_\mu \bar{\nu}_e, \nu_e \bar{\nu}_\tau, \nu_\tau \bar{\nu}_e, \nu_\mu \bar{\nu}_\mu, \nu_\tau \bar{\nu}_\mu, \nu_\tau \bar{\nu}_\tau, E^0 E^0$. The first six combinations are mediated by W^\pm or/and S_1^\pm while those of $E^0 E^0$ are mediated by T^\pm . Here E^0 could be E_1^0 and possibly $E_{2,3}^0$ if it decays into a charged lepton and T^\pm outside the detector. The background is given by the process $E_{miss} \equiv \nu_\mu \bar{\nu}_e$, which occurs in the SM via 18 Feynman diagrams and via 40 diagrams in the present class of models¹³. The total expected cross section and the expected number of events for the processes $e^-e^+ \rightarrow e^-\mu^+ + E_{miss}$ are represented by σ^{EX} and $N^{EX} = \mathcal{L}\sigma^{EX}$, with \mathcal{L} being the integrated luminosity. In the SM case we have $N^B = \mathcal{L}\sigma^B$. As an example, we consider the following benchmark for the KNT case (n=0)¹³

$$\begin{aligned}
f_{e\mu} &= -(4.97 + i1.41) \times 10^{-2}, \quad f_{e\tau} = 0.106 + i0.0859, \quad f_{\mu\tau} = (3.04 - i4.72) \times 10^{-6}, \\
g_{i\alpha} &= 10^{-2} \times \begin{pmatrix} 0.2249 + i0.3252 & 0.0053 + i0.7789 & 0.4709 + i1.47 \\ 1.099 + i1.511 & -1.365 - i1.003 & 0.6532 - i0.1845 \\ 122.1 + i178.4 & -0.6398 - i0.6656 & -10.56 + i68.56 \end{pmatrix}, \\
M_{E_i^0} &= \{162.2 \text{ GeV}, 182.1 \text{ GeV}, 209.8 \text{ GeV}\}, \quad M_{S_1} = 914.2 \text{ GeV}, \quad M_T = 239.7 \text{ GeV} \quad (7)
\end{aligned}$$

We used CalcHEP¹⁴ to simulate the model and generate the differential cross section and the relevant kinematic variables for different CM energy: $E_{CM} = 250, 350, 500$ GeV and 1 TeV, initially with unpolarized beams; and then we consider polarized beams with $P(e^-, e^+) = [-0.8, +0.3]$ and/or $P(e^-, e^+) = [+0.8, -0.3]$. After imposing the appropriate cuts in both cases of polarized and unpolarized beams, we summarize the results for the corresponding luminosity values in Table-1.

In Fig. 3, we show the dependance of the significance on the accumulated luminosity with and without polarized beams for the considered CM energies. We clearly see that for a polarized beam, the signal can be observed even with relatively low integrated luminosity. For example, at $E_{CM} = 250$ GeV, the 5σ required luminosity is 150 fb^{-1} for polarized beam as compared to 700 fb^{-1} without polarization.

E_{CM} (GeV)	L (fb^{-1})	$P(e^-, e^+)$	N_B	N_{EX}	N_S
250	250	0, 0	16480	16851	371
		-0.8, +03	38498	39775	1277
350	350	0, 0	20609	21055	446
		-0.8, +03	47740	48990	1250
500	500	0, 0	28280	28815	535
		-0.8, +03	65500	67250	1750
1000	1000	0, 0	19.217	469.76	450.54
		+0.8, -03	2.07	727.10	725.03

Table 1: The expected (N_{EX}) and background (N_B) number of events for different CM energy values with/without polarized beams within the cuts given in Table-1.

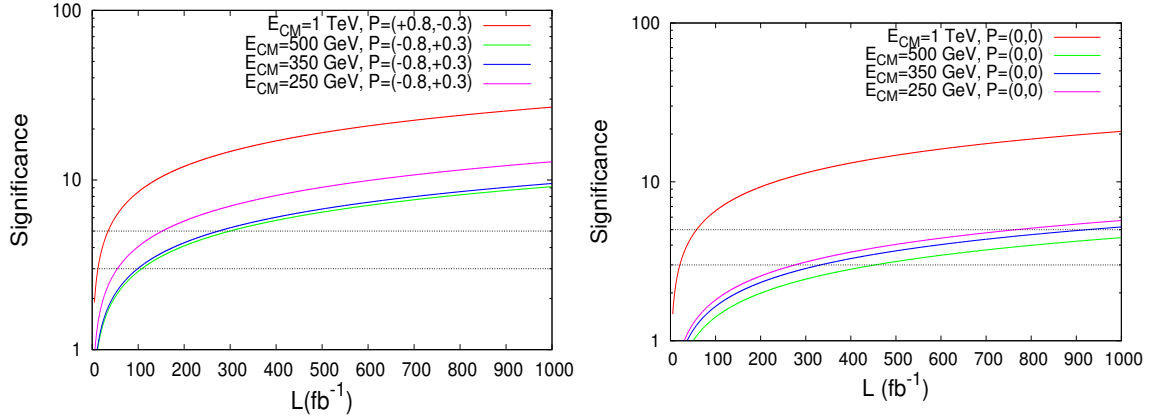


Figure 3: The significance versus luminosity at different CM energies within the cuts defined in Table-1; with (left) and without (right) polarized beams. The two horizontal dashed lines represent $S = 3$ and $S = 5$, respectively.

Turning now to the LHC, the processes $pp \rightarrow e^-e^+ + E_{miss}$, $\mu^-\mu^+ + E_{miss}$, $e^-\mu^+ + E_{miss}$ can be modified with respect to the SM, where the missing energy could correspond to any of the combinations mentioned above. We used CalcHEP¹⁴ to generate different distributions for two CM energies $E_{CM} = 8, 14$ TeV. After selecting the cuts, we obtain the results in Fig. 4, which shows the significance versus the charged scalar mass M_{S_1} for the luminosity values $\mathcal{L} = 20.3$ and 100 fb^{-1} that correspond $E_{CM} = 8, 14$ TeV, respectively¹⁵.

From Fig. 4-left, it is clear that the charged scalar mass should be larger than 780 GeV, and from Fig. 4-right, we conclude that this signal can be seen for LHC14.

6 Conclusion

We have shown that a generalized class of three-loop neutrino mass models offers a promising way to experimentally probe the new physics that is responsible for the origin of neutrino mass. We showed that the models can solve both the neutrino mass and DM problems without being in conflict with LFV constraints such as the severe bound on $B(\mu \rightarrow e\gamma)$ and the muon anomalous magnetic moment. We also investigated possible signatures at both the LHC and ILC through the deviation from the SM in the processes $pp \rightarrow e^-e^+ + E_{miss}$, $\mu^-\mu^+ + E_{miss}$, $e^-\mu^+ + E_{miss}$ and $e^-e^+ \rightarrow e^-\mu^+ + E_{miss}$ respectively. From the recent results of LHC8, we put a bound on the charged scalar mass $M_{S_1} > 780 \text{ GeV}$.

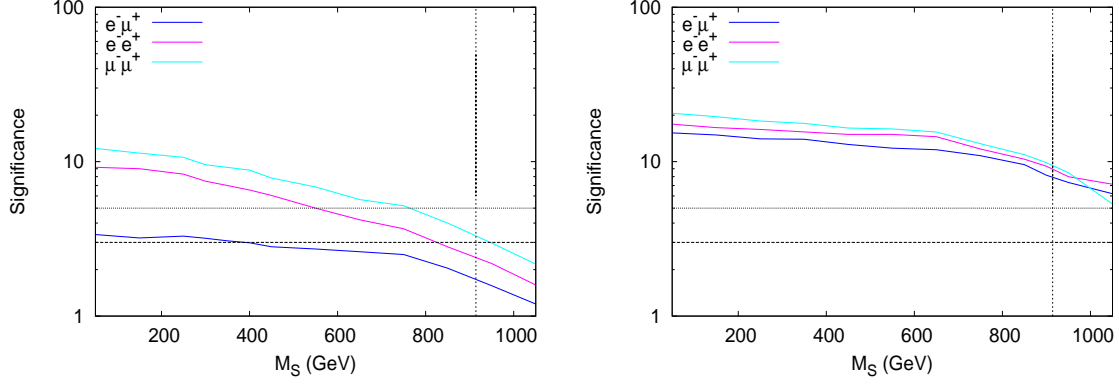


Figure 4: The significance versus the charged scalar mass, M_{S_1} , at the CM energy 8 TeV (left) and 14 TeV (right). The two horizontal dashed lines represent $S = 3$ and $S = 5$, respectively.

Acknowledgments

AA wants to thank the organizers for financial support. The authors thank R. Soualah, C. S. Chen, T. Toma, Ch. Guella and D. Chergui for productive collaborations in this field.

References

1. L. M. Krauss, S. Nasri and M. Trodden, Phys. Rev. D **67**, 085002 (2003).
2. A. Ahriche, C. S. Chen, K. L. McDonald and S. Nasri, Phys. Rev. D **90**, 015024 (2014) [arXiv:1404.2696 [hep-ph]].
3. A. Ahriche, K. L. McDonald and S. Nasri, JHEP **1410**, 167 (2014) [arXiv:1404.5917 [hep-ph]].
4. A. Ahriche, K. L. McDonald, S. Nasri and T. Toma, arXiv:1504.05755 [hep-ph].
5. C. S. Chen, K. L. McDonald and S. Nasri, Phys. Lett. B **734**, 388 (2014) [arXiv:1404.6033 [hep-ph]].
6. G. Aad et al. (ATLAS Collaboration), Phys. Lett. B **716**, 1-29 (2012).
7. S. Chatrchyan et al. (CMS Collaboration), Phys. Lett. B **716**, 30-61 (2012).
8. A. Ahriche and S. Nasri, JCAP **1307**, 035 (2013).
9. J. Adam *et al.* [MEG Collaboration], Phys. Rev. Lett. **110**, 201801 (2013) [arXiv:1303.0754 [hep-ex]].
10. K.A. Olive et al. (Particle Data Group), Chin. Phys. C, **38**, 090001 (2014).
11. D.V. Forero, M. Tortola and J.W.F. Valle, Phys. Rev. D **86**, 073012 (2012).
12. A. Ahriche, Phys. Rev. D **75**, 083522 (2007); A. Ahriche and S. Nasri, Phys. Rev. D **83**, 045032 (2011); Phys. Rev. D **85**, 093007 (2012); A. Ahriche, G. Faisel, S. Y. Ho, S. Nasri and J. Tandean, arXiv:1501.06605 [hep-ph].
13. A. Ahriche, S. Nasri and R. Soualah, Phys. Rev. D **89**, 095010 (2014).
14. A. Belyaev, N. D. Christensen and A. Pukhov, Comput. Phys. Commun. **184** (2013) 1729-1769, arXiv:1207.6082 [hep-ph].
15. C. Guella, et al, 'in progress'.